

Leveraging ultra-low interfacial tension and liquid–liquid phase separation in embedded 3D bioprinting


F SCI


Cite as: Biophysics Rev. 3, 031307 (2022); <https://doi.org/10.1063/5.0087387>

Submitted: 04 February 2022 • Accepted: 23 August 2022 • Published Online: 28 September 2022

 Senthilkumar Duraivel,  Vignesh Subramaniam, Steven Chisolm, et al.

COLLECTIONS

 This paper was selected as Featured

 This paper was selected as Scilight



View Online



Export Citation



CrossMark

ARTICLES YOU MAY BE INTERESTED IN

[Improving 3D bioprinting in liquids](#)

Scilight 2022, 401104 (2022); <https://doi.org/10.1063/10.0014461>

[Multiscale architecture: Mechanics of composite cytoskeletal networks](#)

Biophysics Reviews 3, 031304 (2022); <https://doi.org/10.1063/5.0099405>

[Myocardial infarction from a tissue engineering and regenerative medicine point of view: A comprehensive review on models and treatments](#)

Biophysics Reviews 3, 031305 (2022); <https://doi.org/10.1063/5.0093399>



Read Now!

AIP Advances

Biophysics & Bioengineering Collection

Leveraging ultra-low interfacial tension and liquid-liquid phase separation in embedded 3D bioprinting



Cite as: Biophysics Rev. **3**, 031307 (2022); doi: 10.1063/5.0087387

Submitted: 4 February 2022 · Accepted: 23 August 2022 ·

Published Online: 28 September 2022 · Publisher error corrected: 27 October 2022



View Online



Export Citation



CrossMark

Senthilkumar Duraivel,^{1,a)} Vignesh Subramaniam,^{2,a)} Steven Chisolm,^{2,a)} Georg M. Scheutz,^{3,a)} Brent S. Sumerlin,^{3,a)} Tapomoy Bhattacharjee,^{4,a)} and Thomas E. Angelini^{2,b)}

AFFILIATIONS

¹Department of Materials Science and Engineering, University of Florida, Gainesville, Florida 32611, USA

²Department of Mechanical & Aerospace Engineering, University of Florida, Gainesville, Florida 32611, USA

³George & Josephine Butler Polymer Research Laboratory, Center for Macromolecular Science & Engineering, Department of Chemistry, University of Florida, Gainesville, Florida 32611, USA

⁴National Centre for Biological Sciences, Tata Institute of Fundamental Research, Bellary Road, Bangalore 560065, Karnataka, India

^{a)}Electronic addresses: senthilkduraivel@ufl.edu; v.subramaniam@ufl.edu; stevenchisolm@ufl.edu; gscheutz@chem.ufl.edu; sumerlin@chem.ufl.edu; and tapa@ncbs.res.in

^{b)}Author to whom correspondence should be addressed: t.e.angelini@ufl.edu

ABSTRACT

Many recently developed 3D bioprinting strategies operate by extruding aqueous biopolymer solutions directly into a variety of different support materials constituted from swollen, solvated, aqueous, polymer assemblies. In developing these 3D printing methods and materials, great care is often taken to tune the rheological behaviors of both inks and 3D support media. By contrast, much less attention has been given to the physics of the interfaces created when structuring one polymer phase into another in embedded 3D printing applications. For example, it is currently unclear whether a dynamic interfacial tension between miscible phases stabilizes embedded 3D bioprinted structures as they are shaped while in a liquid state. Interest in the physics of interfaces between complex fluids has grown dramatically since the discovery of liquid-liquid phase separation (LLPS) in living cells. We believe that many new insights coming from this burst of investigation into LLPS within biological contexts can be leveraged to develop new materials and methods for improved 3D bioprinting that leverage LLPS in mixtures of biopolymers, biocompatible synthetic polymers, and proteins. Thus, in this review article, we highlight work at the interface between recent LLPS research and embedded 3D bioprinting methods and materials, and we introduce a 3D bioprinting method that leverages LLPS to stabilize printed biopolymer inks embedded in a bioprinting support material.

Published under an exclusive license by AIP Publishing. <https://doi.org/10.1063/5.0087387>

TABLE OF CONTENTS

I. INTRODUCTION	1
II. INTERFACIAL TENSION IN EMBEDDED 3D PRINTING	3
III. BACKGROUND: RECENT DISCOVERY OF LLPS IN LIVING CELLS.....	3
IV. LEVERAGING LLPS IN 3D BIOPRINTING WITH PROTEIN AND BIOPOLYMER SOLUTIONS.....	5
V. LLPS AND 3D BIOPRINTING WITH BIOPOLYMERS AND SYNTHETIC BIOCOMPATIBLE POLYMERS.....	6

VI. BIOMEDICAL DEVICE FABRICATION: PRINTING WITH SILICONE ELASTOMER AND FLUOROELASTOMER.....	8
VII. CONCLUSION AND OUTLOOK.....	10
VIII. METHODS AND MATERIALS.....	10
A. Fluorescent PEG microgel synthesis and formulation.....	10
B. PDMS/PMPS emulsion and fluorescent PDMS formulation.....	10

I. INTRODUCTION

The ambitious goal of fabricating functional and implantable tissues and organs has motivated the development of numerous

advanced materials and methods for 3D bioprinting.¹ A diversity of innovative strategies have been developed for 3D printing structures made from biopolymers, living cells, and other biomaterials, where a common set of problems arise: these materials most often must be shaped while in a liquid state, they do not rapidly solidify, and after solidification, they are so soft that they cannot hold their own shapes in response to gravitational or interfacial forces.² For example, traditional layer-by-layer extrusion of aqueous polymer solutions onto solid substrates leads to the slumping and spreading of structures unless non-Newtonian rheological modifiers are added to the inks.^{3–5} To sidestep the need for specialized materials, numerous embedded 3D bioprinting approaches have been developed in which living cell populations are shaped while in the liquid state, extruded directly into a support medium that holds nascent structures in place as they slowly solidify and mature.^{6,7} The physical stability provided by the support medium counteracts the otherwise disruptive forces of gravity and interfacial tension. Popular examples of these support materials include jammed microgels,^{6,8–11} packed micelles,^{12,13} and polymer networks with labile bonds.^{14,15} While these embedded 3D printing approaches have been effective for shaping biomaterials and other phases of soft matter, we generally lack a deep understanding of the interfaces between printed inks and their support materials. For example, in embedded 3D printing, it is commonplace to extrude aqueous polymer solutions into packs of aqueous microgels without finding significant mixing between the two phases. Such printed liquid shapes appear to be stable over several hours throughout the process of fabricating large-scale structures. Establishing detailed understanding of these complex fluid interfaces will provide fundamental insight into how current embedded printing methods work and may lead to the development of design principles that facilitate material selection. Additionally, such new understanding would help to guide the development of new materials that intentionally leverage liquid–liquid phase separation (LLPS) for improved embedded 3D printing performance.

In recent years, the physics of fluid interfaces has been intensely studied within the context of liquid–liquid phase separation (LLPS). The resurging interest in LLPS was inspired by its discovery in living cells, where small liquid droplets containing concentrated proteins, nucleic acids, or other biomolecules were shown to play key roles in intracellular signaling processes.^{16–19} The discovery of LLPS in living cells motivated a large breadth of *in vitro* studies of LLPS in purified solutions of proteins, biopolymers, and biocompatible synthetic polymers.^{20–22} Together, this body of work further inspired investigations of LLPS in more complex systems that mimic some aspects of the cells' interior, focusing on cytoskeletal assembly and dynamics,^{23–25} for example, or the elastic resistance to growing liquid droplets within polymer networks.^{26,27} Similar complexities may contribute to the interfacial physics in embedded 3D printing applications, where concentrated polymer solutions are injected into other supporting complex fluids without significant mixing, despite the two phases sharing a solvent—most often, water. Even in cases where the two miscible fluid phases are not in thermodynamic equilibrium with one another, their interfaces may be stabilized by a dynamic interfacial tension, which was first formalized in a theory by Korteweg in 1901²⁸ and studied in many experiments since then.²⁹ Thus, established knowledge of the interfacial physics between miscible fluids may provide a foundation for explaining how numerous examples of embedded 3D printing

work, and along with our recently enriched understanding of LLPS may inspire the development of new embedded 3D printing materials and strategies. One clear benefit of leveraging LLPS in embedded 3D printing is that liquids capable of going through reversible phase separation near room or body temperature often have ultra-low interfacial tension, which could severely reduce the destructive forces that interfacial tension applies to printed features.³⁰ The same benefits are provided by the interfaces between non-equilibrium miscible phases, though the kinetics of diffusive mixing may need to be accounted for. We believe that failing to explore the potential roles of miscible fluid interfaces and LLPS in current and new 3D printing approaches would represent a missed opportunity to leverage a growing base of knowledge in the burgeoning and exciting field of LLPS that could point to new directions in biofabrication.

Given the clear connection between the study of diffusive mixing between separated miscible fluids approaching equilibrium and the reverse process of LLPS, we refer to investigations in these areas generically as “LLPS research” throughout this manuscript, though we specify the different scenarios when needed. In this brief review, we discuss work that represents the interface between LLPS research and embedded 3D bioprinting methods and materials. Given the large breadth of published work in both areas, we restrict our focus to research in each field that may be relevant to the other. To set the stage, we begin by describing how using LLPS as a strategy for embedded 3D bioprinting may surmount current limitations on the minimum diameter of features that will remain stable after printing (Sec. II). We follow this motivating section with a brief review of the foundational work on LLPS in living cells (Sec. III). We discuss *in vitro* research on LLPS in mixtures of protein or biopolymer solutions and commonly used crowding agents like polyethylene glycol (PEG) and dextran (Sec. IV). Given the popularity of PEG and dextran in this field of work, we also review LLPS studies in pure mixtures of PEG and dextran, along with LLPS studies involving comparable biocompatible synthetic polymers (Sec. V). We highlight a few examples where the LLPS strategy is already intentionally employed in 3D printing applications. The final area we review relates to silicone and fluorocarbon materials that are employed in biomedical applications; these materials are used to make scaffolding for cells and to fabricate biomedical devices (Sec. VI). For example, there is a rich body of work on LLPS in silicone polymer blends that are yet to be leveraged in embedded 3D printing methods to create structures from silicone elastomer. We conclude this brief review by proposing future directions that current knowledge in LLPS and embedded 3D bioprinting could enable. Throughout this review, we include brief illustrative experimental results that demonstrate the feasibility of the methods we introduce, so we include Sec. VIII.

Finally, we note that the primary focus of this brief review article is not printing mimics of the biological condensates described in Sec. III. By contrast, we include Sec. III in the manuscript to briefly review the discovery of LLPS in living cells and highlight later progress in the area. Our purpose for including this section is to introduce this groundbreaking and relatively new area of discovery to those performing bioprinting with biocompatible polymers, hoping to create excitement about LLPS as an untapped physical principle to be leveraged in embedded 3D printing, more generally. Indeed, the discovery of LLPS in cells led to an expansion of activity in the study of LLPS in purified polymer systems that do not always exhibit the exotic properties of

biological condensates. Thus, we hope that by reviewing these different areas of research, the current momentum in these fields will lead investigators to consider 3D bioprinting as a potential application of their fundamental discoveries.

II. INTERFACIAL TENSION IN EMBEDDED 3D PRINTING

In embedded 3D printing, the interfacial tension between linear extruded features and the supporting media that surrounds them can generate several different types of instability that drive the features to breakup into small droplets, buckle, or coil.³⁰ In addition to interfacial tension, these instabilities are controlled by the yield stresses of the two phases and by the diameter of the extruded features. For example, to prevent the breakup of cylindrical liquid features embedded in a support medium having a finite yield stress, features must be printed having radii larger than γ/σ_y , where γ is the interfacial tension and σ_y is the yield stress of the support medium. While tests of this feature-size limit using pure materials like neat silicone oils and lab-synthesized microgels validated this prediction,³⁰ it is challenging to interpret results where commercially available silicone inks like Sylgard 184 were employed; commonly used filler materials like silica nanoparticles in commercial polydimethylsiloxane (PDMS) formulations likely stabilize the interface between printed structures and support materials, reducing the interfacial tension. The accumulation of fluorescent particles at the interfaces between PDMS inks and support media indicates the potential stabilizing effects of such particulate additives.¹⁰ Still, general trends across different systems are consistent with the role played by interfacial tension. In one example, where Sylgard 184 was printed into a commercial aqueous carbomer, the smallest feature diameter reported was 150 μm .³¹ Reducing this interfacial tension by using a support medium made from micro-organogels swollen in mineral oil, the smallest stable feature diameter reported was 80 μm .¹⁰ Contrasting these examples with experiments where aqueous polymer inks were printed into aqueous support media and in which interfacial tension is expected to be orders of magnitude lower, features with diameters of 20 μm were produced, apparently limited by the relative translation speed of the printing nozzle and the volumetric ink deposition rate, rather than interfacial tension.³² Taken together, these results suggest that developing embedded 3D printing methods in which the interfacial tension between the ink and the support medium is reduced will correspondingly reduce the minimum stable feature size that can be printed, potentially eliminating interfacial tension as a limiting factor in printing quality.

While the disruptive role of interfacial tension in embedded 3D printing has been recognized and investigated,^{30,33} and strategies have been taken to reduce interfacial forces between printed inks and their surrounding support materials,¹⁰ these efforts were limited to material-pairs having high interfacial tension and are immiscible under typical printing conditions. As described in the previous paragraph, these pairs of inks and support materials were aqueous–oil and oil–oil systems. By contrast, interfacial instabilities appear to be eliminated in embedded 3D printing of aqueous inks into aqueous support materials; we have not seen reports of spontaneous breakup of printed features in aqueous–aqueous systems, indicating that the effects of interfacial tension are eliminated when the polymer species constituting the inks and support materials are prepared in the same solvent–water in this case. For example, structures with fine features and intricate detail, made from polyacrylamide (pAAM), polyethylene

glycol (PEG), hyaluronic acid (HA), alginate, and polyvinyl alcohol (PVA), exhibit long-term stability, even without cross-linking after printing into jammed carbomer microgels swollen in water.¹¹ These printing processes were carried out at very low Reynolds' number, $Re \approx 10^{-4}$, where miscible fluid interfaces are smooth and mechanically stable as species diffuse between the two phases. Experiments on diffusive transport across miscible fluid interfaces show that the diffusion coefficients in such scenarios can be as small as seven orders of magnitude smaller than their values in dilute conditions.³⁴ Thus, the combination of ultra-low interfacial tension and slow molecular transport may explain the high-quality of embedded 3D printing processes when using miscible material pairs. It will be interesting in the future to examine how employing jammed solvated microgels as the outer phase, instead of a polymer solution, may contribute to the slowing of diffusive mixing across the interfaces.

While miscible polymer pairs in embedded 3D printing methods may form dynamic stabilizing interfaces between inks and their support materials, their thermodynamic instability represents a kinetic limitation. However, the separation between these material pairs can be made thermodynamically stable with careful formulation. Over wide ranges of polymer concentration and molecular weight, a diversity of biocompatible polymer pairs can be formulated to undergo LLPS at an upper critical solvation temperature (UCST) close to room temperature,³⁵ and the separate phases often have extremely low interfacial tension. For example, phase-separated mixtures of PEG and dextran are reported to have interfacial tensions between 0.0005 and 0.7 mN/m.^{36–43} Thus, while LLPS itself is driven by a thermodynamic instability, it may be leveraged to perform a critical *stabilizing* role in embedded 3D printing, helping to maintain ultra-low interfacial tension interfaces between printed inks and their surrounding support materials, indefinitely. Thus, we are inspired to intentionally leverage the physics of LLPS, moving forward, in developing new embedded 3D printing material pairs. This combination of LLPS and embedded 3D printing is illustrated in Fig. 1. By performing embedded 3D printing at temperatures and compositions that lay below the binodal line, equilibrium structures may be printed where no net-flux of molecules occurs over time. This process would require mixing some fraction of the two polymers into each phase, though the relative concentrations can be quite small. For example, mixtures composed of 6% (w/w) PEG (*m.w.* = 7000 Da) and 8% (w/w) dextran (*m.w.* = 510 000 Da) phase separate, where the PEG-rich phase is composed of 9.9% PEG and only 0.06% dextran (w/w); the dextran rich phase is composed of 19.1% dextran and only 0.52% PEG (w/w).⁴³ It will be useful in the future to investigate the contribution from jammed support media like microgels in such strategies, where the polymers constituting the microgels are solvated but cannot diffuse into the inks and where ink permeability into the microgels is sterically impeded.

III. BACKGROUND: RECENT DISCOVERY OF LLPS IN LIVING CELLS

The first published demonstration of LLPS in living cells occurred in 2009, motivated by the goal of understanding how the reproductive cells in developing organisms localize to one end of embryos at extremely early stages of development. The model organism studied was *Caenorhabditis elegans* (*C. elegans*), a mm-scale nematode worm. Inside the one-cell embryo of these model worms, P-granules—RNA and protein-rich aggregates dispersed in the

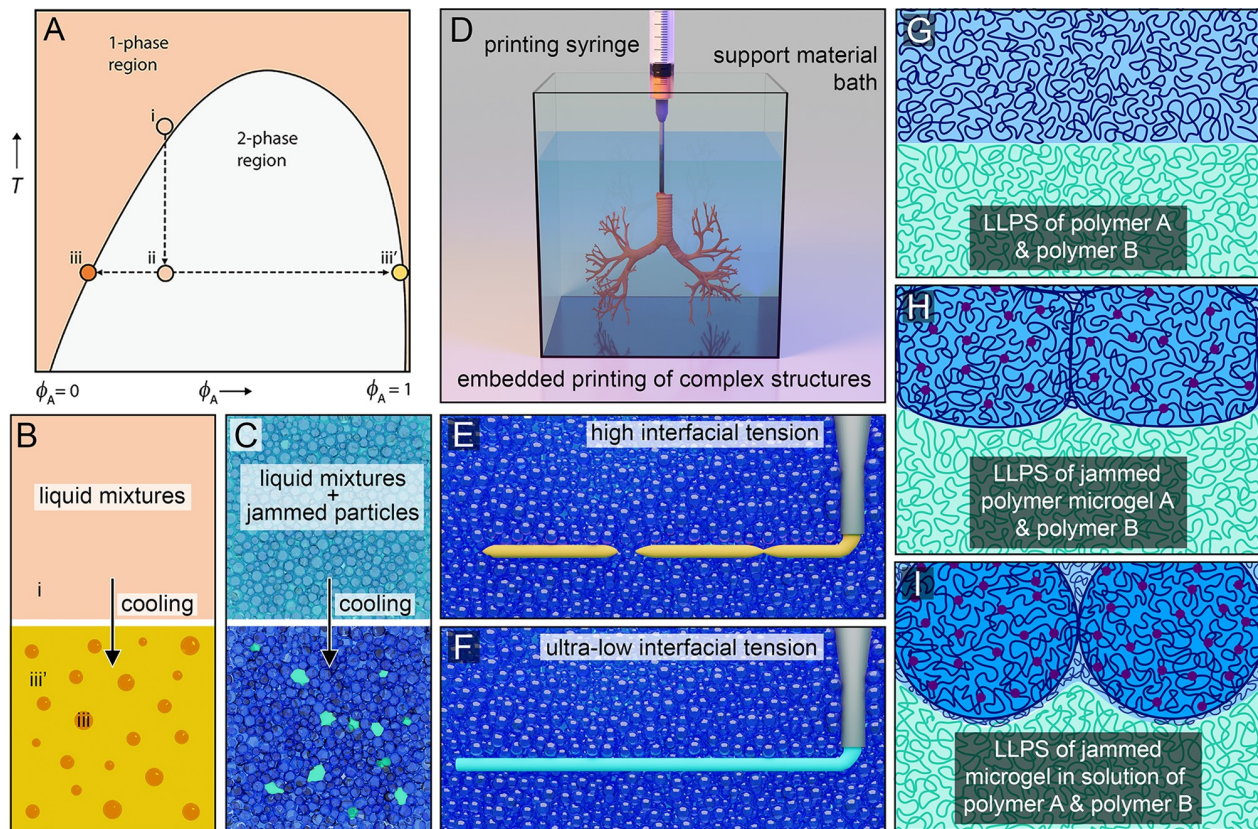


FIG. 1. LLPS and embedded 3D bioprinting. (a) The phase diagram of a polymer blend with an upper critical solution temperature (UCST) is understood; quenching from a stable point (i) to an unstable point at a lower temperature (ii) drives phase separation into a component B rich phase (iii) and a component A rich phase (iii'), where ϕ_A is the concentration of component A and T is the temperature. (b) In this example, a liquid blend separates into a continuous phase rich in component A, and a droplet phase rich in component B. (c) If this blend was the continuous phase of a jammed pack of particles, the phase separated droplets should become trapped in the pore space. (d) If an ink made from component B was printed into a jammed support material permeated by component A at a temperature below the UCST, the phases should remain separate. (e) High interfacial tension between inks and support materials drives feature breakup in embedded 3D printing. (f) Embedded printing with materials that exhibit LLPS and a UCST slightly higher than the printing temperature will exhibit ultra-low interfacial tension and remain stable. (g) While LLPS-assisted embedded 3D printing can be achieved with liquids, mechanical stability can be achieved by combining LLPS with jammed support materials; both conforming hydrogel particles with very little pore space (h) and spherical hydrogel particles permeated by an additional polymer solution (i) may be formulated to serve this purpose.

cytoplasm—were observed to localize to the posterior of the cell, eventually leading to the localization of the reproductive cells at the posterior region of the organism. Although nucleoplasm and cytoplasm contain many macromolecular structures like P-granules, such objects were traditionally thought to be solid, stable structures, hence the term “granule.” Similar to traditional organelles, these structures perform many important functions in the cell, but unlike traditional organelles, they are not encased by a membrane. How these membraneless organelles form and acquire their distinct shapes remained a mystery until Brangwynne *et al.* demonstrated that P-granules are droplets of RNA–protein mixtures that remain phase separated from the cytoplasm and exhibit liquid-like behaviors including fusion, dripping, and wetting. Moreover, their locations inside cells were shown to be governed by their rates of assembly and disassembly, which has striking similarities to condensation and evaporation. Thus, this assembly and disassembly of proteins pointed toward a temporal

phase change that regulates where P granules will form and was ultimately described as a type of LLPS. These findings mark a significant milestone in our understanding of how membraneless organelles are dynamically localized and transported inside cells in the form of phase-separated liquid condensates. A rich body of investigation of these liquid condensates in cells rapidly followed. For example, it was found that the interactions between RNA and RNA–helicase proteins increase molecular transport close to the droplet phase boundary of P-granules and are necessary for the formation and maintenance of P-granules. Furthermore, interactions between RNA and proteins also regulate the physical properties of these P-granules; the viscosity of P-granules increases with increasing RNA concentration, indicating how intracellular liquid-phase organelles achieve tunable material properties.⁴⁴ In such condensates, integrated RNA-binding capacity of protein–interaction networks determines whether LLPS occurs upon RNA

influx. Through similar mechanisms in a diversity of eukaryotic cells, many RNA-dependent membraneless organelles have been found to coexist and interact with each other.^{45–47} Recently, a quantitative reconstitution of cytoplasmic stress granules (SGs) with attached P-bodies revealed a simple stoichiometry-dependent competition between different complexes of RNA binding domains that determine SG and P-body composition and miscibility (Fig. 2).⁴⁸

Similar to the membraneless organelles in cytoplasm, nucleoplasm also contains regions that are not encased by membranes and play critical roles in cell function. For example, nucleoli are membraneless organelles whose main function is ribosome biosynthesis and assist in rapid cell growth; the size and shape of nucleoli are used as indicators of cancer growth and malignancy. Recent exploration of amphibian oocytes reveals that their nucleoli behave as liquid-like droplets of RNA and protein, which regulates their distinct size and shape.⁴⁹ Additional complexities are found in nucleoli, as these membraneless organelles are inhomogeneous structures with internal sub-compartments.^{50–52} For example, sub-compartments within nucleoli are found to exhibit distinct, coexisting, structures of liquid phases that perform different functions during rRNA processing in an assembly-line-like fashion.^{50,53} Such multiphase structures enable different processing steps to occur at different locations while their liquid-like nature facilitates the fast transport of their products between different sub-compartments. Together, these investigations established that LLPS plays a critical role in cellular function, which drove a renaissance in LLPS research and inspired the study of LLPS in complex contexts that expand far beyond its study in simple *in vitro* model polymer systems.

IV. LEVERAGING LLPS IN 3D BIOPRINTING WITH PROTEIN AND BIOPOLYMER SOLUTIONS

The several manifestations of LLPS within living cells point toward leveraging the same basic principles to create large-scale complex structures from proteins and other biopolymers for advanced bio-fabrication applications. We can envision creating inks having the same molecular compositions of P-granules, stress granules, or nucleoli and printing them into environments that mimic those within the cell where they self-assemble. Such 3D printed structures could be used to re-create the “assembly-line” processing and ultimate production of specific biomolecules, as occurs in nucleoli for example, but designed for optimal throughput in macroscopic engineered systems. Such structures could be manufactured to have extremely fine features and high surface area to volume ratios, since the interfacial tension between the phase-separated inks and the surrounding support materials is expected to fall within the range of 10^{-7} and 10^{-5} N/m.^{53–55} We note that the specific ways to leverage the phenomena of LLPS within cells for 3D bioprinting applications are currently unclear and represent an unexplored frontier. For example, by controlling LLPS with specific sequences of proteins and nucleic acids and employing by non-equilibrium processes like transcription, a diversity of new and highly tunable strategies in 3D bioprinting could be developed.

While such applications that recapitulate complex intracellular processes in large-scale *in vitro* scaffolding are speculative at this stage, the principles of LLPS in neurodegenerative processes could be leveraged more readily. Protein condensates and Lewy-body formation are key factors behind multiple neurodegenerative diseases;⁵⁶ many of such assemblies have liquid like properties and are membraneless. For example, α -synuclein (α -Syn) condensation and subsequent amyloid

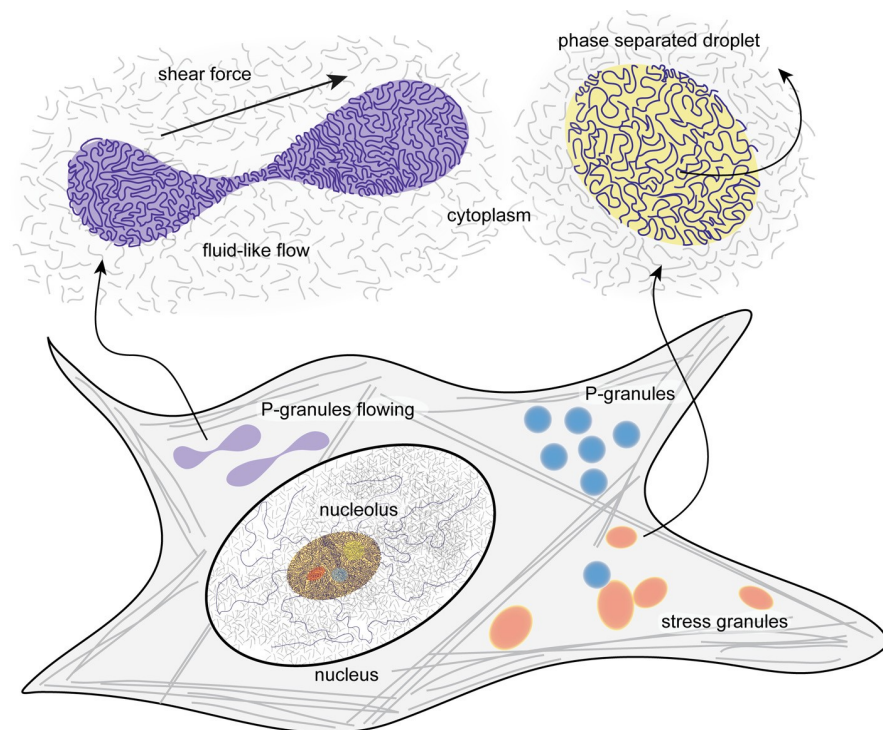


FIG. 2. Both the nucleoplasm and cytoplasm contain liquid condensates of biomacromolecules, including P-granules, stress granules, and nucleoli. These “granular” objects were previously thought to be solid, stable structures, but recent investigations have shown that they are phase-separated liquid droplets that exhibit physical characteristics of fluid droplets like dripping when sheared, wetting to surfaces, and the ability to fuse with one another. Much like traditional organelles, these structures perform many important functions in the cell, but unlike traditional organelles, they are not encased by a membrane.

formation are directly linked with Parkinson's disease pathogenesis.⁵⁷ Recent reports have found that LLPS of α -Syn generates liquid-like droplets which eventually undergo a liquid-to-solid transition and form an amyloid hydrogel that contains oligomers and fibrillar species.^{58,59} Similarly, LLPS causes molecular crowding of amyloid-promoting elements of the Alzheimer-related protein, tau, and drives electrostatic coacervation.⁶⁰ Investigations of the interplay between different proteins like tau and α -synuclein in LLPS are elucidating the interconnection between different neurodegenerative diseases. Recent studies have found that the accumulation of α -Syn into tau-associated condensates can contribute to synergistic α -Syn/tau pathologies.⁶¹ Overall, the well-established role of LLPS in neurodegenerative disease indicates that using the embedded 3D printing strategy outlined in Fig. 1 would be effective at creating *in vitro* models for studying degenerative processes with a high degree of control over key factors like geometric complexity, kinetics of molecular transport, and spatially heterogeneous composition.

Expanding beyond neurodegenerative disease, a broader diversity of proteins exhibit LLPS in the presence of molecular crowders like PEG, dextran, and Ficoll, which are used to mimic the steric aspects of the intracellular microenvironment.⁶² Extracellular matrix (ECM) proteins like collagen⁶³ and gelatin⁶⁴ have also been compartmentalized using an LLPS-based approach. In all these cases, it may be possible to leverage LLPS in embedded 3D printing strategies in which protein "ink" solutions and a complementary support medium are both prepared at compositions that will remain phase separated throughout the printing process, allowing the ink to remain in a liquid state until printing is complete. Alternatively, non-equilibrium solutions that mix sufficiently slowly through diffusion across their interfaces could be used. This approach may have been unintentionally taken in recent embedded 3D bioprinting work where collagen solutions were extruded into packed microgel support media, both in the presence and absence of living cells.^{7,65} In both these examples, after the collagen self-assembled into a branched network structure, a well-defined interface between the supporting microgel medium and the collagen network was observed. Such an interface would be expected if a dynamic interfacial tension was preserving a defined interface between the materials; if the phases were rapidly mixing, one would expect a more graded interface to form throughout the fairly long gelation process, which takes approximately 30 min to complete. Indeed, in the absence of any compartmentalization, when colonies of actively migrating living objects such as bacteria are 3D printed into similar support materials, the surface profiles of the printed colonies are highly irregular and evolve rapidly.^{66,67}

V. LLPS AND 3D BIOPRINTING WITH BIOPOLYMERS AND SYNTHETIC BIOCOMPATIBLE POLYMERS

In Sec. IV, we attempted to lay out a path for leveraging LLPS in 3D bioprinting of protein-based structures. The same approach could be taken with a broader diversity of materials that are popular components of bioinks, including various large molecular-weight flexible polymers like hyaluronic acid, alginate, dextran, Ficoll, and biocompatible synthetic polymers like PEG and pAAM.^{9,11,13,39,41,68–74} In combination, these polymers can be made to undergo LLPS at ambient 3D printing conditions. The most common pair of polymers used to create a phase separated aqueous system is PEG and dextran. Both polymers are biocompatible, and their phase separation has been studied since at least the 1960s.^{36,43,75–78} Thus, we can leverage the

long history of PEG–dextran and other pairs of biocompatible polymers like Ficoll–dextran, Ficoll–PEG, dextran–gelatin, and pAAM–carboxymethyl cellulose to select materials for bioprinting applications and to develop new pairs of phase-separating polymers for bioprinting. In all these systems, critical control parameters have been investigated, reporting sensitivity of LLPS to temperature, molecular weight, polymer concentration, polymer charge density, pH, interfacial tension, and density differences between separate phases.^{36–38,42,77–80} We envision that the details provided in these manuscripts will help as a valuable starting point for developing LLPS-assisted 3D bioprinting materials.

Previous demonstrations of printing high molecular weight flexible biopolymers into a jammed support material showed excellent results in terms of print fidelity, complexity, and stability of printed structures for long periods of time; we hypothesize that these results were facilitated by an ultra-low dynamic interfacial tension.¹¹ In these previous demonstrations, polymer solutions were printed into a support medium made from jammed Carbopol microgels. Such microgels are irregularly shaped and jam at extremely low concentrations, facilitating conformal contact between gel particles, creating an effectively continuous and highly solvated polymer medium that the biopolymer inks may remain separated from for long times after printing. While jammed carbomer appears to remain separated from high-molecular weight polymer inks after printing, as illustrated in Fig. 1(h), our review of LLPS research led us to consider how the addition of a third component could broaden the potential versatility of the concept [Fig. 1(i)]. For example, by mixing spherical PEG microgels with a high molecular weight PEG polymer solution, a more porous support medium may be formulated, compared to packed carbomers. To test this idea, we synthesized fluorescent spherical PEG microgels using inverse emulsion polymerization and mixed them with a 200 kDa molecular weight PEG linear polymer (see Sec. VII). This medium has a shear modulus of approximately 43 Pa and a yield stress of approximately 12 Pa. We printed a solution of fluorescently labeled hyaluronic acid into this medium and examined the resulting structures. Imaging the printed structures at low magnification, we find that the features are well-defined and stable. Imaging at high magnification, we see an interface between the ink and support phases. While the interface appears clear and no mixing was apparent over time, the interface is very rough and seemingly defined by the surface formed by the packed microgels; we expect interfacial forces to be too weak to flatten out the interface, which would require yielding the jammed microgel medium. These results demonstrate that biopolymer solutions can be stably printed into a jammed support medium permeated by a second polymer; microgel jamming serves to stabilize the printed structure while choosing miscible polymer pairs that exhibit a long-timescale interface can ensure that the interfacial tension between the ink and support medium is extremely low (Fig. 3). By formulating these material pairs at the right composition, they may remain phase separated indefinitely, enabled by equilibrium LLPS.

While, in this review, we envision using jammed support media to stabilize structures made from separated liquids in 3D printing applications, the control of fluid interfaces with additional stabilizing agents has been studied for a long time. For example, surfactants, nanoparticles, or polymers can be used to stabilize phase-separated drops to formulate model cells,^{81–85} microgels,⁸⁶ and all-aqueous emulsions.^{87–89} Stabilization is generally sensitive to temperature⁸¹

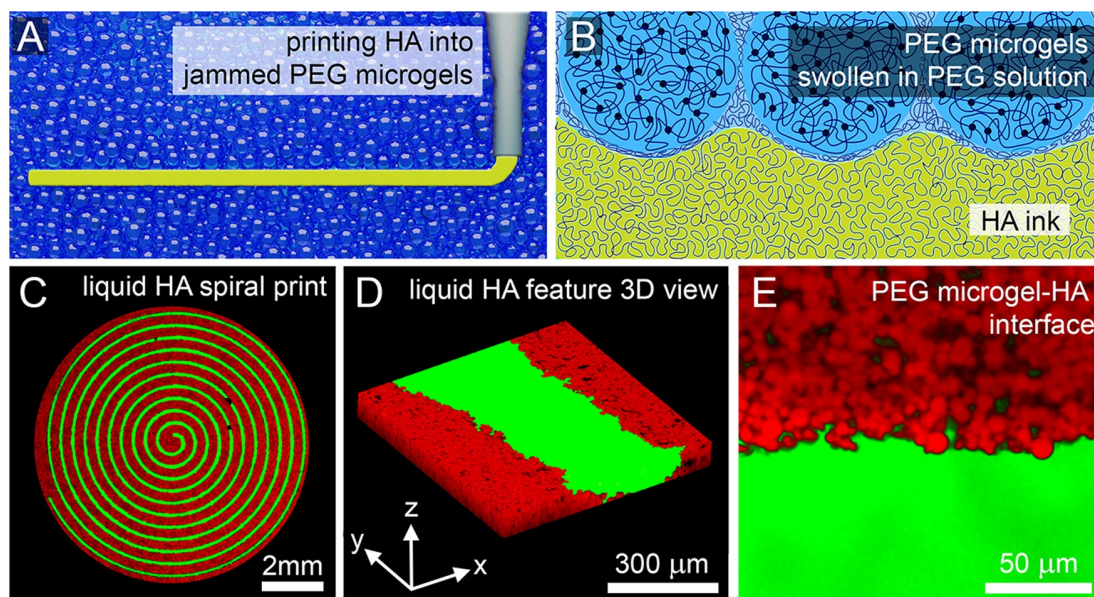


FIG. 3. (a) A jammed pack of spherical PEG microgels can be used as a support medium for 3D bioprinting structures made from biopolymers like hyaluronic acid (HA). (b) To create a continuous interface that the HA ink will remain separated from throughout the printing process, high molecular weight PEG linear polymer is mixed with the PEG microgels. (c) This mixture of PEG microgels with PEG linear polymer provides the physical stability needed to print structures from an HA solution, as shown in low magnification confocal fluorescence microscopy images (green: HA; red: PEG microgels). (d) Higher magnification confocal fluorescence images show a small section of the continuous HA structure surrounded by PEG microgels. (e) High magnification images highlight the interface between the ink and support phases, which is very rough and apparently defined by the surface formed by the packed microgels. The low interfacial tension between HA and PEG solutions appears to be too weak to flatten out the interface, which would require yielding the jammed microgel support medium.

and can also be tuned by leveraging polyelectrolyte complexation, for example using a combination of cationic polydiallyldimethylammonium chloride (PDADMAC) dissolved in PEG and anionic poly(sodium 4-styrenesulfonate) (PSS) dissolved in dextran, where a polyelectrolyte multilayer forms at the interface.⁹⁰ A notable resource for identifying polymer pairs and stabilizing agents can be found in the work by Mace *et al.*,³⁵ where liquid-liquid phase separation in 23 different polymer systems are investigated in over 100 different pairs. These polymers include dextran, Ficoll, polyacrylamide, and PEG, which we have highlighted, and several other polymers, including poly(acrylic acid), hydroxyethyl cellulose, alginate, methyl cellulose, poly(methacrylic acid), poly(vinyl alcohol), polyethyleneimine, and poly(propylene glycol). Higher-order combinations and systems containing surfactants are also reported. These phase separation studies could help in selecting new material pairs with ultra-low interfacial tension suitable for the LLPS-assisted embedded 3D printing strategy proposed here.

The ultra-low interfacial tension concept we propose here has already been captured by some recent demonstrations of polymer-in-polymer 3D printing, sometimes we believe either intentionally or unintentionally. For example, the classic PEG-dextran pair has been used for 3D printing in several studies.^{39–41,91} Although the printed structures in these studies show clean interfaces between the printed inks and the surrounding media, the procedure of printing into a liquid support medium severely limits working time, print fidelity, and microscale complexity, as identified by the studies. Similarly, recent work using an ink composed of a mixture of N-isopropylacrylamide

(NIPAM), bis-acrylamide (BIS), and sodium alginate (NaAlg), printed into a support medium made from aqueous carboxymethyl cellulose (CMC), shows clean interfaces which could potentially be explained by a dynamic interfacial tension between the separate non-equilibrium phases constituting the ink and support material.⁶⁹ Another study describes a method of printing a polylactic-co-glycolic acid (PLGA) solution dissolved in tetraglycol (TG) into water, which acts as an anti-solvent.⁹² Even though this study leverages phase separation for liquid-liquid 3D printing, the mechanism involves precipitation of PLGA after extrusion, driven by the exchange of TG with water. Another strategy is to use engineered polymer systems that transition between fluid and solid-like states, like printing hydrogel inks into a hydrogel matrix, both made of hyaluronic acid with different amounts of repeat units modified with guest-host pairs of adamantane (Ad) and β -cyclodextrin (β -CD).^{14,93} Printed structures with clean interfaces were seen immediately after printing even though the materials are fluidized during the printing process, which could be facilitated by a dynamic interfacial tension between the ink and matrix polymers. A secondary covalent cross-linking mechanism is then used to stabilize the interface between ink and support materials and maintain the printed structures for several days. While, in this review, we focus on inks that do not strongly aggregate, precipitate, or gel during the printing process, but instead remain in the liquid state while remaining separated with a co-solvated support material, we highlight these examples to provide an expanded toolbox for LLPS-mediated 3D printing applications.

As already introduced in this review, an alternative way to achieve ultra-low interfacial tension in embedded 3D bioprinting is to use a jammed phase as a support material, rather than a liquid phase, and to permeate the jammed phase with a miscible polymer solution that exhibits a dynamic interfacial tension with the ink. To test this concept on the PEG–dextran system, we formulated the same PEG–PEG support material described earlier in this section (Fig. 3), printed a fluorescent dextran ink into this medium, and examined the structure. Much like the HA ink, the dextran ink appears continuous and stable from low-magnification images. Imaging at high magnification, we see a clear interface formed between the phases. Also like the HA ink, the dextran ink does not appear to mix with the support medium over time; the interface is very rough and defined by the surface formed by the packed microgels. At the combination of polymer concentrations and molecular weight, used here, the interfacial tension between PEG and dextran is on the order of 0.02 mN/m. Thus, we expect interfacial forces to be too weak to flatten out the interface, which would require yielding the jammed microgel medium. These results represent a second pair of miscible polymer solutions that can be stably printed by synthesizing microgels from the same polymers of at least one of the free-polymer components; microgel jamming serves to stabilize the printed structure, and choosing polymer pairs that exhibit a dynamic interfacial tension can ensure that the interfacial tension between the ink and support medium is extremely low (Fig. 4). By formulating these material pairs at compositions that exhibit equilibrium LLPS, 3D structures could be made stable without diffusive mixing of the phases after printing.

VI. BIOMEDICAL DEVICE FABRICATION: PRINTING WITH SILICONE ELASTOMER AND FLUOROELASTOMER

While most efforts in 3D bioprinting to date have involved some combination of biopolymers and living cells, another critical area is 3D printing of scaffolds and biomedical devices made from polydimethylsiloxane (PDMS) elastomer. PDMS is a versatile material used widely in industrial manufacturing owing to its high thermal stability and resistance to weathering, ozone, moisture, and UV irradiation.^{94–97} These properties, in combination with its biocompatibility, make it an effective material for a diversity of biomedical applications.^{96–98} The difficulties of 3D printing with PDMS-based inks are similar to those encountered with most inks made from complex fluids; 3D printing free-standing structures made from PDMS are excessively challenging without the addition of stabilizing fillers.^{99–102} By contrast, embedded printing of soft PDMS facilitates the fabrication of functional and complex elastomer structures without the need to modify silicone inks.^{10,11,31,103–105} Early examples of jammed particulate support materials for embedded silicone 3D printing include a DOW silicone elastomer blend¹¹ and Carbopol.³¹ In the former case,¹¹ finely detailed structures were printed, exhibiting stability when the ink and the support were both silicone based, likely owing to low interfacial tension between the ink and the support material. When aqueous support materials like Carbopol or oil-in-water emulsions are used, the printed silicone structures have a smooth surface finish,^{31,104} driven by high interfacial tension. However, the disruptive effects of interfacial tension make smooth surface finish and fine stable feature size

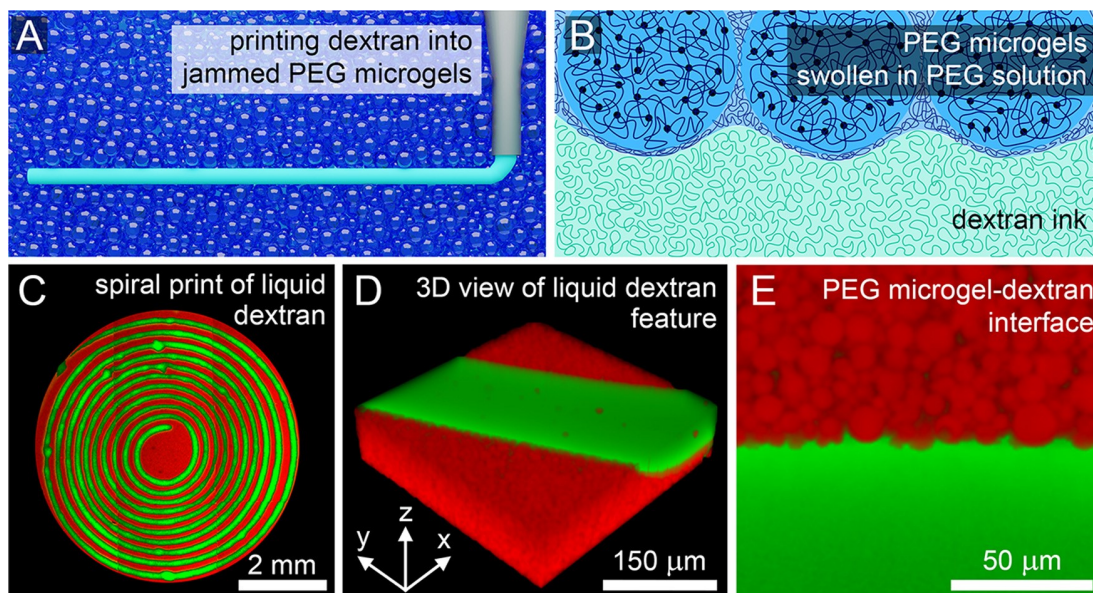


FIG. 4. (a) LLPS in PEG–dextran solutions has been studied thoroughly, facilitating the development of an embedded 3D printing strategy using this pair of polymers. (b) Aiming to print a structure made from dextran solution into a support medium made from PEG, we mixed high molecular weight PEG linear polymer with the PEG microgels, which will create a continuous interface that the dextran ink will separate from throughout the printing process. (c) The PEG microgels provide the physical stability needed to print structures from a dextran while the PEG linear polymers help to maintain a boundary with the dextran ink, as shown in low magnification confocal fluorescence microscopy images (green: dextran; red: PEG microgels). (d) A small section of the continuous dextran structure surrounded by PEG microgels is seen at higher magnification. (e) The interface between the ink and support phase, seen at high magnification, appears rough and apparently defined by the surface formed by the packed microgels. The low interfacial tension between dextran and PEG solutions appears to be insufficient to yield the jammed microgel support medium and flatten the interface.

antagonistic, limiting the feature size that can be achieved and requiring optimization of the print parameters to overcome the feature instability.¹⁰⁵ Recent work investigating different combinations of inks and support materials showed that the interfacial tension and the yield stress of the support material control the minimum stable feature size that can be 3D printed.³⁰ As an intermediate between the extremes of silicone–silicone material pairs and silicone–aqueous material pairs, jammed support materials swollen in hydrocarbon (HC)-based oil enabled printing of stable features having diameters as small as 80 μm , likely associated with a reduced interfacial tension relative to silicone–water pairs.¹⁰ Taken together, this work suggests that using silicone-based inks with silicone-based support materials that exhibit LLPS, having ultra-low interfacial tension, may further improve the quality of printing with PDMS-based inks.

To create a support material that will undergo LLPS with PDMS inks, siloxane polymers having chemical compositions comparable to PDMS need to be employed. One such commercially available candidate is poly(methylphenyl siloxane) (PMPS). PDMS and PMPS phase separation has been studied in detail, revealing the effects of chain length, terminal groups, and chain architecture on the phase boundaries.^{106–110} Linear chains of PDMS and PMPS exhibit a UCST close to room temperature, which can be tuned by varying the molecular weight of each component.¹⁰⁶ Further reduction in the interfacial tension between PDMS and PMPS can be achieved by adding random copolymers of PDMS or PMPS, which helps to stabilize their interfaces.¹¹⁰ Other known polyalkylsiloxanes that undergo phase separation with PDMS include poly(ethylmethyl siloxane) (PEMS)^{111–113} and poly(hexylmethyl siloxane) (PHMS),^{114,115} making them potential candidates for the design of support materials for LLPS-assisted embedded 3D printing of PDMS. One way to make such a support material would be to develop packed particles in a continuum of PMPS, PHMS, or PEMS liquids. For example, microgels that swell in these organosiloxane oils would be excellent candidates for formulating support materials. Once formulated, if the PDMS ink was printed into the support material at a temperature below the UCST, it should remain phase separated but have an ultra-low interfacial tension against the organosiloxane-based support material.

An alternative to microgels as the particulate phase of a jammed support medium is emulsion droplets; an inverse emulsion formulated from aqueous droplets jammed together in a continuous phase made from one of these organosiloxane oils could be used a support material for embedded 3D printing of PDMS structures. To test this idea, we formulated an inverse emulsion of aqueous droplets in a continuous phase made from a 1:1 mixture of 1250 g/mol PDMS oil and 950 g/mol PMPS oil (see Sec. VII). Since the UCST of this PDMS/PMPS mixture is approximately 38 °C, the inverse emulsion was formulated at 46 °C. Dropping the temperature to room temperature, we were able to directly observe LLPS occurring on the microscope [Figs. 5(a) and 5(b)]. Close observation of the samples shows the phase-separated droplets conformally deforming to the shapes of the available pore spaces between the packed emulsion droplets, which we expect because of the low interfacial tension of approximately 2 mN/m between the PDMS and PMPS phases. This jammed emulsion exhibits a shear modulus of 310 Pa and a yield stress of 12 Pa, comparable to previously used support materials, indicating that stable silicone features could be 3D printed into it [Fig. 5(c)]. Thus, to test the suitability of this approach for embedded 3D silicone printing, we extruded a fluorescent

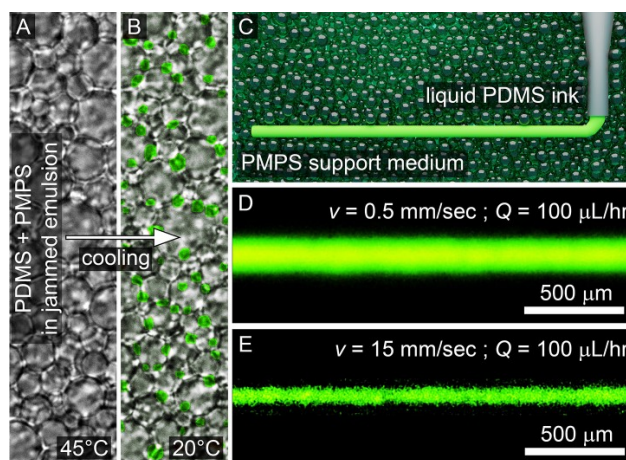


FIG. 5. (a) A PDMS/PMPS polymer blend forms the continuous phase of a jammed aqueous emulsion at temperatures above the UCST of the blend. (b) Below the UCST of the PDMS/PMPS mixture (approximately 38 °C), the continuous phase exhibits LLPS as small droplets appear in the pore-space between emulsion droplets (false coloring). (c) At room temperature, 3D printed structures made from PDMS ink into an aqueous emulsion having PMPS as the continuous phase should remain mechanically stable and transiently separated from the support material. (d) Testing this approach for embedded 3D silicone printing, we extruded a fluorescent PDMS ink into the jammed aqueous/PMPS emulsion. Translating the printing nozzle at lower speeds produced larger diameter features (d) than those produced at higher translation speeds (e). In these preliminary tests, we observed no mixing between the ink and the support medium, and the features were apparently stable over time. As expected, the ink-support interfaces were rough and most likely defined by the surface formed by packed emulsion droplets, given the low interfacial tension between PMPS and PDMS.

PDMS ink into a support material made from jammed aqueous emulsion droplets in a continuous phase of PMPS. By changing the translation speed of the printing nozzle, we were able to control the feature diameter [Figs. 5(d) and 5(e)]. The printed features were found to be stable over time and exhibited no apparent mixing with the support medium, though the interface likely exhibits slow mixing since the two phases were not formulated at equilibrium LLPS compositions. The features exhibited rough interfaces which we believe are defined by the surface formed by packed emulsion droplets, given the low interfacial tension between PMPS and PDMS.

Similar to siloxane polymers, several other non-aqueous polymer mixtures undergo phase separation, and their phase diagrams have been studied with respect to various polymer architecture variables. One such polymer mixture is a blend of hydrocarbon (HC) oil and fluorocarbon oil (FC). Many aspects of liquid–liquid phase separation in HC/FC mixtures have been well studied, including their phase diagrams and the effects of end-groups, chain length, and chain architecture on the corresponding critical temperature.^{116,117} Fluorocarbon-based elastomers (fluoroelastomer) are materials of great interest because of their very high oxygen solubility and resistance to harsh chemicals; the additive manufacturing of fluoroelastomer by embedded 3D printing has not been explored before. By leveraging LLPS of fluoroelastomer precursor oils from hydrocarbon oils, complex shapes of fluoroelastomers can be fabricated by embedded printing into a hydrocarbon-based support system. Support materials for

fluorocarbon printing can be designed by choosing a hydrocarbon oil compatible with a given fluorocarbon ink and by developing a self-assembled organic microgel system swollen in the HC oil, similar to the previous silicone printing approach.¹⁰ Alternatively, jammed emulsions of aqueous droplets in the desired hydrocarbon oil could be used as a support material for fluoroelastomer printing. We envision that fluoroelastomers with customized cross-linking chemistry can be synthesized, and embedded printed structures can be cured under UV or at high temperature. These fabricated fluoroelastomer structures will find applications in the design of complex biomedical devices and scaffolds.

VII. CONCLUSION AND OUTLOOK

Here, we have introduced a 3D bioprinting concept that, in its implementation, could leverage the advances made recently in three dynamic and exciting areas of study: embedded 3D printing, liquid-liquid phase separation within living cells and in the extracellular space, and *in vitro* liquid-liquid phase separation in purified polymer blends. A recent burst of activity in the study of *in vitro* systems was driven by the discovery of LLPS in living cells, and together these areas of investigation have inspired us to consider leveraging the emerging knowledge about LLPS within complex environments to broaden the 3D bioprinting toolbox, and to correspondingly broaden 3D bioprinting applications. The general concept introduced here involves creating support media made from jammed particles embedded in a continuum of polymer solution that has an ultra-low interfacial tension with the printed ink it stabilizes. The interface between phase-separated polymer pairs exhibiting a UCST slightly above the temperature at which printing occurs will exhibit such ultra-low interfacial tension, eliminating the destructive role of interfacial instabilities. To explore the feasibility of this 3D bioprinting concept and to facilitate the development of new 3D bioprinting strategies that leverage this concept, we have briefly reviewed these critical areas of investigation. While many more examples of LLPS and embedded 3D bioprinting exist in the literature, we limited our review to specific cases that are directly relevant to this new 3D bioprinting concept and to the foundational studies of LLPS in living cells to provide context and inspiration to interested researchers.

In this brief review, we described how the discovery of LLPS in living cells and its important role in cell function inspired many *in vitro* investigations of LLPS in systems constituted from combinations of proteins, biopolymers, and synthetic biocompatible polymers. Inspired by the complexity of the intracellular space, studies of LLPS within polymer networks have been performed, revealing a rich interplay between matrix properties and the physics of phase separation. For example, phase separation studies of fluorocarbon oil within an elastic silicone network showed that phase behavior is controlled by the elastic modulus of the surrounding network.^{26,27,118,119} Furthermore, the elastic modulus of the surrounding network was found to inhibit Oswald ripening of phase separated droplets, and the emergence of phase separated droplets were found to stiffen the macroscopic network.^{27,118,119} We believe this reciprocal influence between the material properties of a surrounding matrix and the phase behavior of permeating liquid polymer blends may manifest in other classes of soft matter as well. For example, within the context of this review, the yield-stress of jammed particulate matter may set a limit on the size, rugosity, or coalescence of phase separated droplets that grow in

the pore-space between packed particles. The demonstrated role of jammed microgel yield stress in the stability of embedded fluid structures³⁰ provides a preliminary indication that LLPS within jammed media will exhibit such a rich set of phenomena to investigate, as occurred when studying LLPS in polymer networks. We hope new fundamental investigations of LLPS in jammed materials or other phases of soft matter will be motivated by the LLPS-mediated 3D printing strategy described here, in addition to the inspiration already drawn from the discovery of LLPS within living cells.

VIII. METHODS AND MATERIALS

A. Fluorescent PEG microgel synthesis and formulation

To synthesize fluorescent PEG microgels, a solution of 25% (w/w) poly(ethylene glycol) methyl ether acrylate ($M_n = 480 \text{ g mol}^{-1}$), 0.4% (w/w) poly(ethylene glycol) diacrylate ($M_n = 700 \text{ g mol}^{-1}$), 0.5% (w/w) methacryloxyethyl thiocarbamoyl rhodamine B, and 0.15% (w/w) ammonium persulfate is prepared in ultrapure water. Separately, a 0.7% (w/w) polyglycerol polyricinoleate (a commercial surfactant) solution is prepared in kerosene. The aqueous and organic solutions are then combined in a beaker, placed on an ice bath, and homogenized at 8000 rpm for 5 min to form a milky-white emulsion. Nitrogen is bubbled through the covered solution for 1 h to displace dissolved oxygen. The deoxygenated reaction mixture is removed from ice and transferred to a 1 l round bottom flask equipped with a magnetic stirring bar. At this time, 0.5% (w/w) of 1,2-di(dimethylamino)ethane (TEMED) is added dropwise while the solution is stirred in a nitrogen atmosphere for 1 h. The solution is then exposed to air and stirred for 30 min to complete the reaction. To separate the microgels from the kerosene phase, methanol is added to the microgel solution, and the mixture is vigorously shaken in 500 ml centrifuge tubes followed by centrifugation at 3500 xg for 5 min and removal of supernatant; these washing steps are performed three times to completely remove the surfactant and organic phases. Finally, water is added in place of methanol, and the washing/centrifugation/supernatant removal steps are repeated twice.

To prepare a 3D printing support medium that will exhibit LLPS with hyaluronic acid and dextran inks, we mix the fluorescent PEG microgels with high molecular weight PEG linear polymers ($M_v = 200\,000$). The final PEG linear polymer concentration in the support media for HA printing is 20% (w/w); for dextran printing, the PEG linear polymer concentration is 10% (w/w). Rheological tests were performed using an Anton Paar MCR702 rheometer. To prepare ink solutions for printing, fluorescently labeled (fluorescein) hyaluronic acid was suspended in water at a concentration of 10 mg/ml; fluorescein-dextran was suspended in water at a 10% concentration (w/w).

B. PDMS/PMPS emulsion and fluorescent PDMS formulation

To formulate a support material for embedded printing of silicone, aqueous droplets were homogenized at 5000 rpm within a continuous phase of 10 cSt silicone oil (DMS-T11, Gelest Inc.) at a volume fraction of 75:25 aqueous to oil phase. The aqueous phase consists of a mixture of water and glycerol (99% pure, Fisher) mixed at 49:51 weight ratios, to match the refractive index of the silicone oil phase ($RI_{Si} = 1.399$). The emulsions were stabilized by the addition of surfactant (DOWSIL ES-5600, Dow) at 1% (w/w) relative to the total emulsion weight. For the phase separation studies of PDMS and

PMPS (PMM-0021, Gelest Inc.) oils within the packed emulsion system, PMPS was mixed with the PDMS based inverse emulsion at 50 °C in such a way that the final emulsion continuous phase has 1:1 weight ratio of PDMS and PMPS oils.

To formulate a fluorescently labeled PDMS ink for printing, fluorescein (2.00 g, 6.02 mmol), cystamine dihydrochloride (4.07 g, 18.1 mmol), 4-dimethylaminopyridine (DMAP; 0.222 g, 1.81 mmol), and ethylcarbodiimide hydrochloride (EDC-HCl, 3.46 g, 18.1 mmol) were combined in a flame dried round bottom flask under Argon (Ar). At 0 °C, dry DMF (30 ml) was added followed by triethylamine (TEA; 5.0 ml, 36 mmol). The reaction was stirred overnight (16 h) and warmed up to room temperature. The reaction mixture was diluted with methanol (MeOH; 15 ml) and DI water (15 ml), and the pH was adjusted to 7 with aqueous HCl (1 M). Dithiothreitol (5.0 g, 32 mmol) was added under Ar, and the reaction was stirred overnight (12 h). Upon acidification with aqueous HCl (1 M) to a pH of 3, the product precipitated from the reaction mixture. After centrifugation and drying *in vacuo*, Fluo-SH was obtained as a red solid (0.82 g; 2.0 mmol; 33% yield) and used without further purification.

Vinyl-terminated PDMS (MW = 28 000 g/mol, Gelest, Inc., 2.5 g, 0.089 mmol) and 2,2-dimethoxy-2-phenylacetophenone (DMPA, 0.002 mg, 0.009 mmol) were dissolved in THF (15 ml) in a round bottom flask. Fluo-SH (0.28 g, 0.71 mmol) was added in DMF (0.5 ml), and the solution was sparged with Ar for 15 min. Subsequently, the thiol-ene reaction was initiated with UV light. After 4 h stirring in the UV light, the reaction was exposed to oxygen, and the solution was diluted with methanol, causing a phase separation with PDMS in the bottom layer. The PDMS layer was collected, and residual solvent was removed on the rotovap. The crude product was re-dissolved in hexanes (5 ml), and the solution was filtered through a syringe filter (0.45 μ m) to remove any precipitates. This cycle of methanol-induced phase separation followed by filtration in hexanes was repeated three times until the methanol supernatant remained clear. The final product Fluo-PDMS was obtained after drying *in vacuo* overnight.

ACKNOWLEDGMENTS

The authors would like to thank Anton Paar for use of their rheometer through the Anton Paar VIP research program.

AUTHOR DECLARATIONS

Conflict of Interest

The authors have no conflicts to disclose.

Author Contributions

S.D. and V.S. contributed equally to this work.

Senthilkumar Duraivel: Conceptualization (equal); Investigation (equal); Methodology (equal); Writing – original draft (equal); Writing – review & editing (equal). **Vignesh Subramaniam:** Conceptualization (equal); Investigation (equal); Writing – original draft (equal); Writing – review & editing (equal). **Steven Chisolm:** Investigation (equal); Writing – original draft (equal). **Georg M. Scheutz:** Investigation (equal); Methodology (equal); Writing – original draft (equal). **Brent Sumerlin:** Conceptualization (equal);

Funding acquisition (equal); Supervision (equal); Writing – original draft (equal). **Tapomoy Bhattacharjee:** Conceptualization (equal); Investigation (equal); Writing – original draft (equal); Writing – review & editing (equal). **Thomas Ettore Angelini:** Conceptualization (equal); Funding acquisition (equal); Investigation (equal); Methodology (equal); Project administration (equal); Supervision (equal); Writing – original draft (equal); Writing – review & editing (equal).

DATA AVAILABILITY

The data that support the findings of this study are available from the corresponding author upon reasonable request.

REFERENCES

- I. Matai, G. Kaur, A. Seyedsalehi, A. McClinton, and C. T. Laurencin, *Biomaterials* **226**, 119536 (2020).
- C. S. O'Bryan, T. Bhattacharjee, S. R. Niemi, S. Balachandar, N. Baldwin, S. T. Ellison, C. R. Taylor, W. G. Sawyer, and T. E. Angelini, *MRS Bull.* **42**(8), 571–577 (2017).
- Y. Jin, D. Zhao, and Y. Huang, *Bio-Des. Manuf.* **1**(2), 123–134 (2018).
- Y. Jin, Y. Shen, J. Yin, J. Qian, and Y. Huang, *ACS Appl. Mater. Interfaces* **10**(12), 10461–10470 (2018).
- Y. Jiang, J. Zhou, Z. Yang, D. Liu, X. Xu, G. Zhao, H. Shi, and Q. Zhang, *J. Mater. Sci.* **53**(16), 11883–11900 (2018).
- T. Bhattacharjee, C. J. Gil, S. L. Marshall, J. M. Uruña, C. S. O'Bryan, M. Carstens, B. Keselowsky, G. D. Palmer, S. Ghivizzani, and C. P. Gibbs, *ACS Biomater. Sci. Eng.* **2**(10), 1787–1795 (2016).
- C. D. Morley, S. T. Ellison, T. Bhattacharjee, C. S. O'Bryan, Y. Zhang, K. F. Smith, C. P. Kabb, M. Sebastian, G. L. Moore, and K. D. Schulze, *Nat. Commun.* **10**(1), 3029 (2019).
- T. J. Hinton, Q. Jallerat, R. N. Palchesko, J. H. Park, M. S. Grodzicki, H.-J. Shue, M. H. Ramadan, A. R. Hudson, and A. W. Feinberg, *Sci. Adv.* **1**(9), e1500758 (2015).
- Y. Jin, A. Compaan, T. Bhattacharjee, and Y. Huang, *Biofabrication* **8**(2), 025016 (2016).
- C. S. O'Bryan, T. Bhattacharjee, S. Hart, C. P. Kabb, K. D. Schulze, I. Chilakala, B. S. Sumerlin, W. G. Sawyer, and T. E. Angelini, *Sci. Adv.* **3**(5), e1602800 (2017).
- T. Bhattacharjee, S. M. Zehnder, K. G. Rowe, S. Jain, R. M. Nixon, W. G. Sawyer, and T. E. Angelini, *Sci. Adv.* **1**(8), e1500655 (2015).
- W. Wu, A. DeConinck, and J. A. Lewis, *Adv. Mater.* **23**(24), H178–H183 (2011).
- M. Rocca, A. Fragasso, W. Liu, M. A. Heinrich, and Y. S. Zhang, *SLAS Technol.* **23**(2), 154–163 (2018).
- C. B. Highley, C. B. Rodell, and J. A. Burdick, *Adv. Mater.* **27**(34), 5075–5079 (2015).
- C. B. Rodell, A. L. Kaminski, and J. A. Burdick, *Biomacromolecules* **14**(11), 4125–4134 (2013).
- C. P. Brangwynne, C. R. Eckmann, D. S. Courson, A. Rybarska, C. Hoeger, J. Gharakhani, F. Jülicher, and A. A. Hyman, *Science* **324**(5935), 1729–1732 (2009).
- Y. Shin and C. P. Brangwynne, *Science* **357**(6357), eaaf4382 (2017).
- C. P. Brangwynne, P. Tompa, and R. V. Pappu, *Nat. Phys.* **11**(11), 899–904 (2015).
- T. Yoshizawa, R.-S. Nozawa, T. Z. Jia, T. Saio, and E. Mori, *Biophys. Rev.* **12**(2), 519–539 (2020).
- Q. Li, X. Peng, Y. Li, W. Tang, J. a Zhu, J. Huang, Y. Qi, and Z. Zhang, *Nucleic Acids Res.* **48**(D1), D320–D327 (2020).
- S. Deshpande and C. Dekker, *Curr. Opin. Colloid Interface Sci.* **52**, 101419 (2021).
- C. Roden and A. S. Gladfelter, *Nat. Rev. Mol. Cell Biol.* **22**(3), 183–195 (2021).

- ²³D. R. Scheff, K. L. Weirich, K. Dasbiswas, A. Patel, S. Vaikuntanathan, and M. L. Gardel, *Soft Matter* **16**(24), 5659–5668 (2020).
- ²⁴K. L. Weirich, S. Banerjee, K. Dasbiswas, T. A. Witten, S. Vaikuntanathan, and M. L. Gardel, *Proc. Natl. Acad. Sci.* **114**(9), 2131–2136 (2017).
- ²⁵K. L. Weirich, K. Dasbiswas, T. A. Witten, S. Vaikuntanathan, and M. L. Gardel, *Proc. Natl. Acad. Sci.* **116**(23), 11125–11130 (2019).
- ²⁶R. W. Style, T. Sai, N. Fanelli, M. Ijavi, K. Smith-Mannschott, Q. Xu, L. A. Wilen, and E. R. Dufresne, *Phys. Rev. X* **8**(1), 011028 (2018).
- ²⁷K. A. Rosowski, T. Sai, E. Vidal-Henriquez, D. Zwicker, R. W. Style, and E. R. Dufresne, *Nat. Phys.* **16**, 422–425 (2020).
- ²⁸D. J. Korteweg, *Arch. Néerl. Sci. Exactes Nat.* **6**, 1–24 (1901).
- ²⁹D. Truzzolillo and L. Cipelletti, *Soft Matter* **13**(1), 13–21 (2017).
- ³⁰C. S. O'Bryan, A. Brady-Mine, C. J. Tessmann, A. M. Spotz, and T. E. Angelini, *Soft Matter* **17**(14), 3886–3894 (2021).
- ³¹T. J. Hinton, A. Hudson, K. Pusch, A. Lee, and A. W. Feinberg, *ACS Biomater. Sci. Eng.* **2**(10), 1781–1786 (2016).
- ³²C. S. O'Bryan, T. Bhattacharjee, S. L. Marshall, W. G. Sawyer, and T. E. Angelini, *Bioprinting* **11**, e00037 (2018).
- ³³E. Pairam, H. Le, and A. Fernández-Nieves, *Phys. Rev. E* **90**(2), 021002 (2014).
- ³⁴S. E. May and J. V. Maher, *Phys. Rev. Lett.* **67**(15), 2013–2016 (1991).
- ³⁵C. R. Mace, O. Akbulut, A. A. Kumar, N. D. Shapiro, R. Derda, M. R. Patton, and G. M. Whitesides, *J. Am. Chem. Soc.* **134**(22), 9094–9097 (2012).
- ³⁶D. Forciniti, C. Hall, and M. Kula, *J. Biotechnol.* **16**(3–4), 279–296 (1990).
- ³⁷E. Atefi, J. A. Mann, Jr., and H. Tavana, *Langmuir* **30**(32), 9691–9699 (2014).
- ³⁸Y. Liu, R. Lipowsky, and R. Dimova, *Langmuir* **28**(8), 3831–3839 (2012).
- ³⁹D. Petrak, E. Atefi, L. Yin, W. Chilian, and H. Tavana, *Biotechnol. Bioeng.* **111**(2), 404–412 (2014).
- ⁴⁰H. Tavana, B. Mosadegh, and S. Takayama, *Adv. Mater.* **22**(24), 2628–2631 (2010).
- ⁴¹G. Luo, Y. Yu, Y. Yuan, X. Chen, Z. Liu, and T. Kong, *Adv. Mater.* **31**(49), 1904631 (2019).
- ⁴²H. Kusumaatmaja, Y. Li, R. Dimova, and R. Lipowsky, *Phys. Rev. Lett.* **103**(23), 238103 (2009).
- ⁴³J. Ryden and P.—a. Albertsson, *J. Colloid Interface Sci.* **37**(1), 219–222 (1971).
- ⁴⁴S. Elbaum-Garfinkle, Y. Kim, K. Szczepaniak, C. C.-H. Chen, C. R. Eckmann, S. Myong, and C. P. Brangwynne, *Proc. Natl. Acad. Sci.* **112**(23), 7189–7194 (2015).
- ⁴⁵K. H. Shah, S. N. Varia, L. A. Cook, and P. K. Herman, *PLoS One* **11**(6), e0158776 (2016).
- ⁴⁶S. L. Moon, T. Morisaki, A. Khong, K. Lyon, R. Parker, and T. J. Stasevich, *Nat. Cell Biol.* **21**(2), 162–168 (2019).
- ⁴⁷N. Kedersha, G. Stoeklin, M. Ayodele, P. Yacono, J. Lykke-Andersen, M. J. Fritzler, D. Scheuner, R. J. Kaufman, D. E. Golan, and P. Anderson, *J. Cell Biol.* **169**(6), 871–884 (2005).
- ⁴⁸D. W. Sanders, N. Kedersha, D. S. Lee, A. R. Strom, V. Drake, J. A. Riback, D. Bracha, J. M. Eeftens, A. Iwanicki, and A. Wang, *Cell* **181**(2), 306–324.e28 (2020).
- ⁴⁹C. P. Brangwynne, T. J. Mitchison, and A. A. Hyman, *Proc. Natl. Acad. Sci.* **108**(11), 4334–4339 (2011).
- ⁵⁰F.-M. Boisvert, S. van Koningsbruggen, J. Navascués, and A. I. Lamond, *Nat. Rev. Mol. Cell Biol.* **8**(7), 574–585 (2007).
- ⁵¹S. Jain, J. R. Wheeler, R. W. Walters, A. Agrawal, A. Barsic, and R. Parker, *Cell* **164**(3), 487–498 (2016).
- ⁵²A. Hubstenberger, S. L. Noble, C. Cameron, and T. C. Evans, *Dev. Cell* **27**(2), 161–173 (2013).
- ⁵³M. Feric, N. Vaidya, T. S. Harmon, D. M. Mitrea, L. Zhu, T. M. Richardson, R. W. Kriwacki, R. V. Pappu, and C. P. Brangwynne, *Cell* **165**(7), 1686–1697 (2016).
- ⁵⁴L. M. Jawerth, M. Ijavi, M. Ruer, S. Saha, M. Jahnel, A. A. Hyman, F. Jülicher, and E. Fischer-Friedrich, *Phys. Rev. Lett.* **121**(25), 258101 (2018).
- ⁵⁵M. Ijavi, R. W. Style, L. Emmanouilidis, A. Kumar, S. M. Meier, A. L. Torzynski, F. H. Allain, Y. Barral, M. O. Steinmetz, and E. R. Dufresne, *Soft Matter* **17**(6), 1655–1662 (2021).
- ⁵⁶A. Zbinden, M. Pérez-Berlanga, P. D. Rossi, and M. Polymenidou, *Dev. Cell* **55**(1), 45–68 (2020).
- ⁵⁷N. M. Kanaan, C. Hamel, T. Grabinski, and B. Combs, *Nat. communications* **11**(1), 2809 (2020).
- ⁵⁸S. Ray, N. Singh, R. Kumar, K. Patel, S. Pandey, D. Datta, J. Mahato, R. Panigrahi, A. Navalkar, and S. Mehra, *Nat. Chem.* **12**(8), 705–716 (2020).
- ⁵⁹M. C. Hardenberg, T. Sinnige, S. Casford, S. T. Dada, C. Poudel, E. A. Robinson, M. Fuxreiter, C. F. Kaminski, G. S. Kaminski Schierle, and E. A. Nollen, *J. Mol. Cell Biol.* **13**(4), 282–294 (2021).
- ⁶⁰S. Ambadipudi, J. Biernat, D. Riedel, E. Mandelkow, and M. Zweckstetter, *Nat. Commun.* **8**(1), 275 (2017).
- ⁶¹A. Siegert, M. Rankovic, F. Favretto, T. Umkar-Godec, T. Strohäker, S. Becker, and M. Zweckstetter, *Protein Sci.* **30**(7), 1326–1336 (2021).
- ⁶²A. A. André and E. Spruijt, *Int. J. Mol. Sci.* **21**(16), 5908 (2020).
- ⁶³S. Singh and H. Tavana, *Front. Chem.* **6**, 379 (2018).
- ⁶⁴Y. Xu, R. Qi, H. Zhu, B. Li, Y. Shen, G. Krainer, D. Klenerman, and T. P. Knowles, *Adv. Mater.* **33**(33), 2008670 (2021).
- ⁶⁵Y. Zhang, S. T. Ellison, S. Duraivel, C. D. Morley, C. R. Taylor, and T. E. Angelini, *Bioprinting* **21**, e00121 (2021).
- ⁶⁶T. Bhattacharjee, D. B. Amchin, R. Alert, J. Ott, and S. S. Datta, *arXiv:2101.04576* (2021).
- ⁶⁷T. Bhattacharjee, D. B. Amchin, J. A. Ott, F. Kratz, and S. S. Datta, *Biophys. J.* **120**, 3483 (2021).
- ⁶⁸D. Chahal, A. Ahmadi, and K. C. Cheung, *Biotechnol. Bioeng.* **109**(11), 2932–2940 (2012).
- ⁶⁹T. Uchida and H. Onoe, *Micromachines* **10**(7), 433 (2019).
- ⁷⁰L. A. Hockaday, K. H. Kang, N. W. Colangelo, P. Y. C. Cheung, B. Duan, E. Malone, J. Wu, L. N. Girardi, L. J. Bonassar, H. Lipson, C. C. Chu, and J. T. Butcher, *Biofabrication* **4**(3), 035005 (2012).
- ⁷¹N. E. Fedorovich, J. R. De Wijn, A. J. Verbout, J. Alblas, and W. J. A. Dhert, *Tissue Eng., Part A* **14**(1), 127–133 (2008).
- ⁷²I. T. Ozbolat and M. Hospodiuk, *Biomaterials* **76**, 321–343 (2016).
- ⁷³A. Skardal, J. Zhang, L. McCoard, X. Xu, S. Oottamasathien, and G. D. Prestwich, *Tissue Eng., Part A* **16**(8), 2675–2685 (2010).
- ⁷⁴A. G. Teixeira, R. Agarwal, K. R. Ko, J. Grant-Burt, B. M. Leung, and J. P. Frampton, *Adv. Healthcare Mater.* **7**(6), 1701036 (2018).
- ⁷⁵P. Å. Albertsson, *Partition of Cell Particles and Macromolecules: Distribution and Fractionation of Cells, Viruses, Microsomes, Proteins, Nucleic Acids, and Antigen-Antibody Complexes in Aqueous Polymer Two-Phase Systems* (Wiley, 1960).
- ⁷⁶P.-Å. Albertsson, *Adv. Protein Chem.* **24**, 309–341 (1970).
- ⁷⁷D. Forciniti, C. Hall, and M.-R. Kula, *Fluid Phase Equilib.* **61**(3), 243–262 (1991).
- ⁷⁸V. Cesi, B. Kitzbauer, M. Narodoslawsky, and A. Moser, *Int. J. Thermophys.* **17**(1), 127–135 (1996).
- ⁷⁹M. W. Edelman, E. Van Der Linden, and R. H. Tromp, *Macromolecules* **36**(20), 7783–7790 (2003).
- ⁸⁰M. Vis, V. F. Peters, R. H. Tromp, and B. H. Erné, *Langmuir* **30**(20), 5755–5762 (2014).
- ⁸¹M. S. Long, C. D. Jones, M. R. Helfrich, L. K. Mangeney-Slavin, and C. D. Keating, *Proc. Natl. Acad. Sci.* **102**(17), 5920–5925 (2005).
- ⁸²C. D. Keating, *Acc. Chem. Res.* **45**(12), 2114–2124 (2012).
- ⁸³N. Martin, *ChemBioChem* **20**(20), 2553–2568 (2019).
- ⁸⁴W. M. Aumiller, Jr. and C. D. Keating, *Adv. Colloid Interface Sci.* **239**, 75–87 (2017).
- ⁸⁵C. D. Crowe and C. D. Keating, *Interface Focus* **8**(5), 20180032 (2018).
- ⁸⁶S. Mytnyk, A. G. Olive, F. Versluis, J. M. Poolman, E. Mendes, R. Eelkema, and J. H. van Esch, *Angew. Chem.* **129**(47), 15119–15123 (2017).
- ⁸⁷S. D. Hann, K. J. Stebe, and D. Lee, *ACS Appl. Mater. Interfaces* **9**(29), 25023–25028 (2017).
- ⁸⁸J. Esquena, *Curr. Opin. Colloid Interface Sci.* **25**, 109–119 (2016).
- ⁸⁹Y. Chao and H. C. Shum, *Chem. Soc. Rev.* **49**(1), 114–142 (2020).
- ⁹⁰S. D. Hann, T. H. Niepa, K. J. Stebe, and D. Lee, *ACS Appl. Mater. Interfaces* **8**(38), 25603–25611 (2016).
- ⁹¹G. Xie, J. Forth, Y. Chai, P. D. Ashby, B. A. Helms, and T. P. Russell, *Chem* **5**(10), 2678–2690 (2019).
- ⁹²A. V. Mironov, O. A. Mironova, M. A. Syachina, and V. K. Popov, *Polymer* **182**, 121845 (2019).

- ⁹³K. H. Song, C. B. Highley, A. Rouff, and J. A. Burdick, *Adv. Funct. Mater.* **28**(31), 1801331 (2018).
- ⁹⁴S. C. Shit and P. Shah, *Nat. Acad. Sci. Lett.* **36**(4), 355–365 (2013).
- ⁹⁵F. J. Schoen, *ASAIO J.* **37**(2), 44–48 (1991).
- ⁹⁶V. R. Sastri, *Plastics in Medical Devices: Properties, Requirements, and Applications* (William Andrew, 2021).
- ⁹⁷M. Zare, E. R. Ghomi, P. D. Venkatraman, and S. Ramakrishna, *J. Appl. Polym. Sci.* **138**, 50969 (2021).
- ⁹⁸V. Ozbolat, M. Dey, B. Ayan, A. Povilianskas, M. C. Demirel, and I. T. Ozbolat, *ACS Biomater. Sci. Eng.* **4**(2), 682–693 (2018).
- ⁹⁹P. Huang, Z. Xia, and S. Cui, *Mater. Des.* **142**, 11–21 (2018).
- ¹⁰⁰L.-y. Zhou, Q. Gao, J.-z. Fu, Q.-y. Chen, J.-p. Zhu, Y. Sun, and Y. He, *ACS Appl. Mater. Interfaces* **11**(26), 23573–23583 (2019).
- ¹⁰¹L. Y. Zhou, J. Fu, and Y. He, *Adv. Funct. Mater.* **30**(28), 2000187 (2020).
- ¹⁰²B. M. Rauzan, A. Z. Nelson, S. E. Lehman, R. H. Ewoldt, and R. G. Nuzzo, *Adv. Funct. Mater.* **28**(21), 1707032 (2018).
- ¹⁰³J. T. Muth, D. M. Vogt, R. L. Truby, Y. Mengüç, D. B. Kolesky, R. J. Wood, and J. A. Lewis, *Adv. Mater.* **26**(36), 6307–6312 (2014).
- ¹⁰⁴K. Hajash, B. Sparrman, C. Guberan, J. Laucks, and S. Tibbits, *3D Printing Addit. Manuf.* **4**(3), 123–132 (2017).
- ¹⁰⁵S. Abdollahi, A. Davis, J. H. Miller, and A. W. Feinberg, *PLoS One* **13**(4), e0194890 (2018).
- ¹⁰⁶C. M. Kuo and S. J. Clarson, *Macromolecules* **25**(8), 2192–2195 (1992).
- ¹⁰⁷C. M. Kuo, S. J. Clarson, and J. A. Semlyen, *Polymer* **35**(21), 4623–4626 (1994).
- ¹⁰⁸C. M. Kuo and S. J. Clarson, *Eur. Polym. J.* **29**(5), 661–664 (1993).
- ¹⁰⁹C. M. Kuo and S. J. Clarson, *Polymer* **41**(15), 5993–6002 (2000).
- ¹¹⁰A. Stammer and B. A. Wolf, *Macromol. Rapid Commun.* **19**, 123–126 (1998).
- ¹¹¹H. Horiuchi, S. Irie, and T. Nose, *Polymer* **32**(11), 1970–1974 (1991).
- ¹¹²S. Enders, A. Stammer, and B. Wolf, *Macromol. Chem. Phys.* **197**(9), 2961–2972 (1996).
- ¹¹³D. Chopra, M. Kontopoulou, D. Vlassopoulos, and S. G. Hatzikiriakos, *Can. J. Chem. Eng.* **80**(6), 1057–1064 (2002).
- ¹¹⁴A. R. Imre, T. Kraska, and L. V. Yelash, *Phys. Chem. Chem. Phys.* **4**(6), 992–1001 (2002).
- ¹¹⁵A. Stammer and B. A. Wolf, *Polymer* **39**(10), 2065–2067 (1998).
- ¹¹⁶P. Lo Nostro, *Adv. Colloid Interface Sci.* **56**, 245–287 (1995).
- ¹¹⁷P. Lo Nostro, a L. Scalise, and P. Baglioni, *J. Chem. Eng. Data* **50**(4), 1148–1152 (2005).
- ¹¹⁸J. Y. Kim, Z. Liu, B. M. Weon, T. Cohen, C.-Y. Hui, E. R. Dufresne, and R. W. Style, *Sci. Adv.* **6**(13), eaaz0418 (2020).
- ¹¹⁹R. W. Style, R. Boltyanskiy, B. Allen, K. E. Jensen, H. P. Foote, J. S. Wettlaufer, and E. R. Dufresne, *Nat. Phys.* **11**(1), 82–87 (2014).